

Metal-Free Flat Lens Using Negative Refraction by Nonlinear Four-wave Mixing

Jianjun Cao¹, Yuanlin Zheng¹, Yaming Feng¹, Xianfeng Chen¹, and Wenjie Wan^{1,2*}

¹The State Key Laboratory of Advanced Optical Communication Systems and Networks, Department of Physics and Astronomy, Shanghai Jiao Tong University, Shanghai 200240, China

²University of Michigan-Shanghai Jiao Tong University Joint Institute, Shanghai 200240, China

A perfect lens with unlimited resolution has always posed a challenge to both theoretical and experimental physicists. Recent developments in optical meta-materials promise an attractive approach towards perfect lenses using negative refraction to overcome the diffraction limit, improving resolution. However, those artificially engineered meta-materials usually company by high losses from metals and are extremely difficult to fabricate. An alternative proposal on using negative refraction by four-wave mixing has attracted much interests recently, though most of existing experiments still require metals and none of them has been implemented for an optical lens. Here we experimentally demonstrate a metal-free flat lens for the first time using negative refraction by degenerate four-wave mixing with a simple thin glass slide. We realize optical lensing utilizing a nonlinear refraction law, which may have potential applications in infrared microscopy and super-resolution imaging.

Flat lenses using negative refraction create a new avenue for novel optical imaging applications, attracting intense interests from optics, microwave and even acoustic communities. Unlike traditional optical lenses, a flat lens can bend incoming waves at negative angles opposed to those within normal refraction regime [1-3]; moreover, it has the ability to negatively refract waves at all-angle including the evanescent ones, making itself a “perfect lens” to overcome the diffraction limit [4]. Such lenses have been realized in many formats ranging from optics to microwave, including photonic crystals [5, 6], metal thin film [4], meta-material [6-10], etc. However, most of them suffer from high losses in association with metallic materials, i.e. the key elements bringing in negative permittivity and artificial permeability. Secondly, fabrications of such nano/micro structures raise additional obstacle for their practical applications. In nonlinear optics, alternative approaches to achieve negative refraction have been proposed including phase conjugation, time reversal and four wave mixing (4WM) [3,11,12]. As contrast to those artificially

engineered methods with meta-materials or photonic crystals creating spatial dispersion for negative refraction using linear composition of different materials, nonlinear optics explores nonlinear wave mixings with right angle matching schemes to fulfill the requirements for negative refraction. Principally, only a thin flat nonlinear slab is required. Up to now, such negative refractions using wave mixing have been realized in some thin films with high nonlinearity such as metal and graphite thin film [13-15]. However, due to low nonlinear conversion efficiency and materials' optical transparency, few experiments have been reported for imaging with such nonlinear geometry.

In this letter, we experimentally demonstrate a metal-free flat lens using negative refraction by degenerate four-wave mixing with a simple thin glass slide. A multi-color imaging scheme is realized at millimeter scale by converting original infrared beams into negative refracted visible ones through nonlinear wave mixings inside glass slides containing third-order nonlinearity. Phase matching condition in degenerate four-wave mixing enables the negative refraction of the 4WM beam to the probe beam at some special regimes, while slight phase mismatch can permit a cone of beams with the similar frequencies to undergo negative refraction, focus and form an image. We also study collinear / non-collinear configurations in order to enhance the resolution of images. This new imaging technique may offer new platform for diffraction-free super-resolution microscopy applications in the near future.

In a degenerate 4WM scheme, an intense pump beam at frequency ω_1 and a probe beam at frequency ω_2 incident on a material with third order nonlinear susceptibility $\chi^{(3)}$, generating a 4WM wave at frequency $\omega_3=2\omega_1 - \omega_2$. Their corresponding phases should satisfy the phase matching condition: $k_3=2k_1 - k_2$ to ensure efficient wavelength conversion. With a thin slab material, its thickness can also affect 4WM processes, allowing 4WM with mismatch phases [16]. Moreover, if the slab's thickness is shorter than the wavelength, only partial phase matching is required in case of surface plasmons excitations [13,17-18], nonlinear dark-field microscope [19]. In our experiment, the pump beam at ω_1 incidents on a thin glass slide normally and the probe beam at ω_2 (signal beam carrying the original image) incidents from angle θ_2 , as shown in Fig. 1(a). The angle of the generated 4WM wave is denoted as θ_3 , measured with respect to the surface normal in counter-clockwise direction, which is negative opposed to normal refraction through a thin glass. The phase mismatch of the 4WM process is

$$\Delta k = 2k_1 - k_2 - k_3, \quad (1)$$

where $k_i = \frac{2\pi n_i}{\lambda_i}$ ($i = 1, 2, 3$) are the wave vectors of the pump, the probe and 4WM beams respectively.

The n_i are the refractive indexes in medium. To generate efficient 4WM wave, phase matching condition ($\Delta k = 0$) should be satisfied, which leads to

$$2k_1 = k_2 \cos\theta_2^m + k_3 \cos\theta_3^m, \quad (2)$$

$$k_2 \sin \theta_2^m = -k_3 \sin \theta_3^m, \quad (3)$$

where θ_2^m and θ_3^m are the angles in the medium. These two angles are related to the angles in air by Snell's law:

$$\sin \theta_2 = n_2 \sin \theta_2^m, \quad (4)$$

$$\sin \theta_3 = n_3 \sin \theta_3^m. \quad (5)$$

Equation (3) indicates that the 4WM wave is refracted negatively with respect to the incident probe beam. Insert Eqs. (4) and (5) into Eq. (3), the effective refractive index of the negative refraction effect is obtained in a Snell-like nonlinear refraction law [13] :

$$n_{eff} = \frac{\sin \theta_2}{\sin \theta_3} = -\frac{\lambda_2}{\lambda_3}, \quad (6)$$

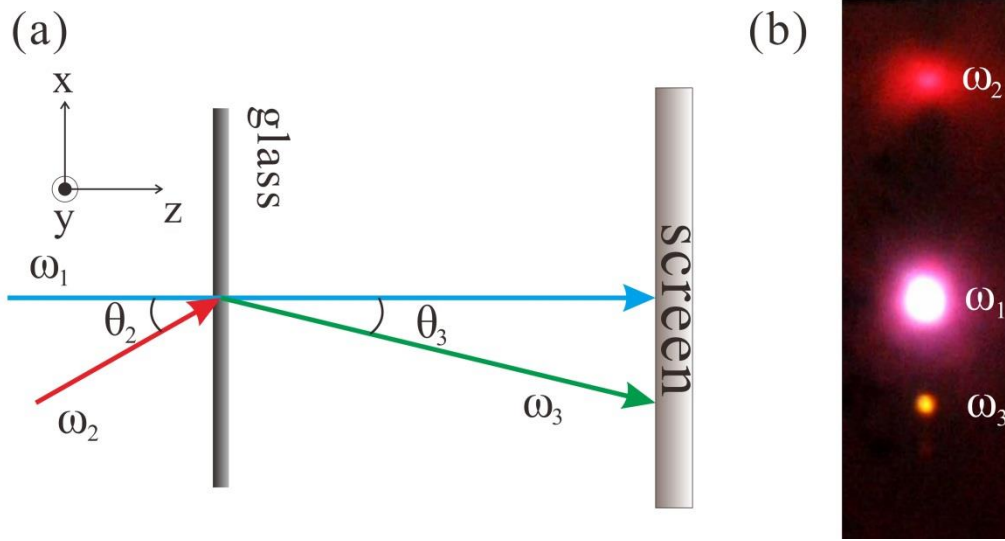


FIG. 1 (a) Schematic of negative refraction effect by degenerate 4WM in a planar glass slide. The pump beam at frequency ω_1 incidents normally on the glass slide mixes with the probe beam at frequency ω_2 to generate 4WM wave at frequency $2\omega_1 - \omega_2$. The 4WM beam exhibits negative refraction relative to the probe beam. (b) Color image on the IR viewing card. The transmitted probe beam at $\lambda_2 = 1300 \text{ nm}$ and the generated 4WM beam at $\lambda_3 = 578 \text{ nm}$ are located on the opposite side of the screen.

In our experiments, the pump beam is delivered by a Ti:Sapphire femtosecond laser source with the pulse duration of $\sim 75 \text{ fs}$ and central wavelength $\lambda_1 = 800 \text{ nm}$. An optical parametric amplifier provides pulses of similar duration at wavelength $\lambda_2 = 1300 \text{ nm}$ as the probe beam. A 1 mm thick BK7 glass slide is used as the nonlinear material. The laser beams incident on the glass slide using geometry in Fig. 1(a), and a delay line is added to ensure the pulses' time overlapping.

The generated 4WM waves after the beams passing through the glass slide are shown in Fig. 1(b). It is obviously to see that the generated 4WM beam is negatively refracted with respect to the input probe beam, located on the opposite sides centered with the pump beam. The incident angle θ_2 is 7.9° and the refracted angle θ_3 is -3.4° . By time-delaying the probe beam, the 4WM intensity varies within 165 fs time frame (see supplement), confirming that ω_3 is generated by nonlinear process. The polarization of the 4WM beam is also measured to be linearly polarized in x direction, the same as the input beams (see supplement). All of

them ensure us the key step of using negative refraction for imaging by 4WM.

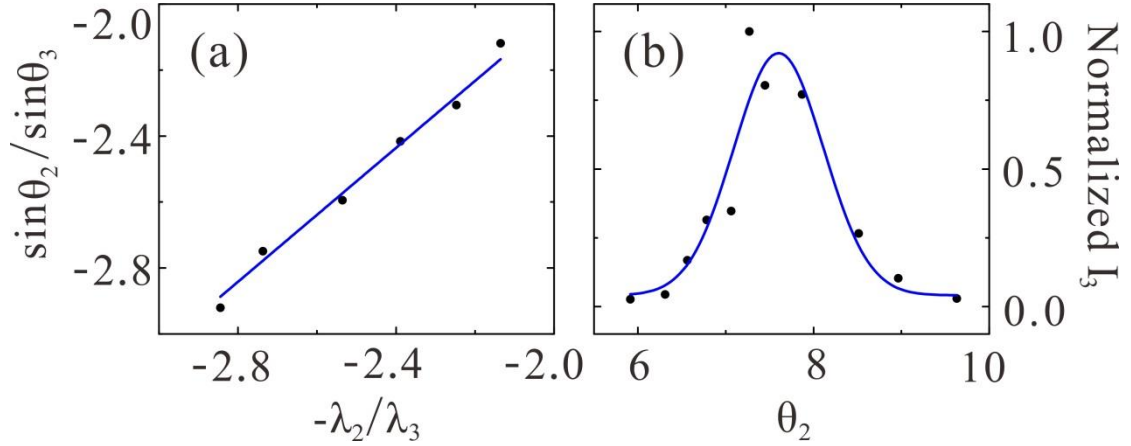


FIG. 2 (a) Nonlinear refraction law. The relationship between $\frac{\sin\theta_2}{\sin\theta_3}$ and $-\frac{\lambda_2}{\lambda_3}$ is plotted with the slope of 1.01 for the linear fitting. (b) The intensity of 4WM wave as a function of excitation angle θ_2 . The dots are measured 4WM intensities for probe beam at wavelength $\lambda_2 = 1300nm$. The solid curve is a Gaussian fitting.

According to the nonlinear refraction law we derived in Eq. (6), the refracted 4WM beam's angle linearly depends on its wavelength. Our experiment measurements confirm this linear relationship between $\frac{\sin\theta_2}{\sin\theta_3}$ and $-\frac{\lambda_2}{\lambda_3}$ to have the exact slope of unit in Fig. 2(a), when varying the incident probe's wavelength from 1250nm to 1500nm while fixing other parameters such as the probe beam's angle, the pump beam, etc. Such nonlinear refraction law is the direct consequence of phase matching condition in 4WM. As long as such law holds, we may extend it to a wider band of probe wavelengths accepting larger accepted angles for imaging, enabling a better imaging resolution [19,25]. However, phase matching scheme in our experiment is complicated by the ultrafast pulse's bandwidth and glass slide's thickness. Though exact phase matching only allows 4WM waves to be generated at the exact angle, in real experiment, the ultrafast pulses have finite linewidth $\sim 50nm$ for the pump and $\sim 100nm$ for the probe, allowing 4WMs occur in a small angle spreading cone nearby. For example, in Fig. 2(b), The 4WM intensity reaches its peak at $\theta_2 = 7.6^\circ$, close to the calculated value 7.2° by Eqs. (2) and (3). The width of the peak spreads about $\Delta\theta_2 \approx 1.0^\circ$. Since the nonlinear refraction law in Eq. (6) depicts the linear dependence of wavelength λ to $\sin\theta$, this angle spreading is roughly close to calculated $\sim 0.91^\circ$ spreading calculated with input beams' linewidth accordingly. For imaging applications, such small angle spreading permits multiple rays of beam origin from an object to have their 4WM waves focused on the other side, the key step for an optical lens.

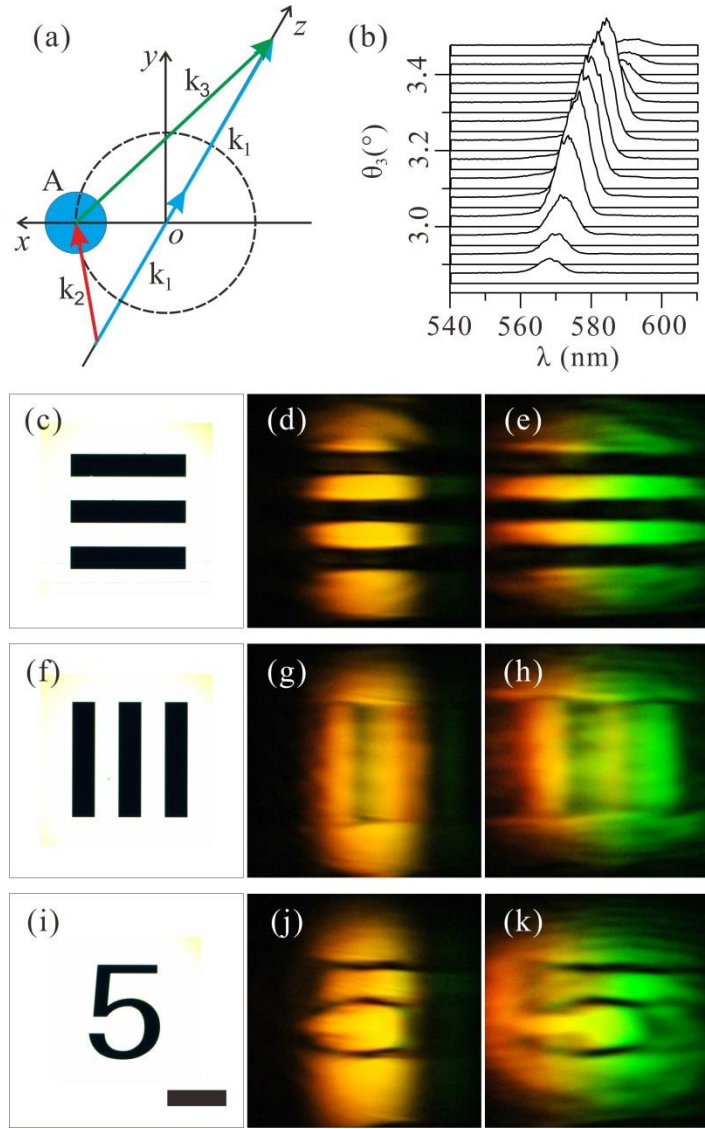


FIG. 3 Imaging a resolution card by nonlinear negative refraction effect in non-collinear configuration. (a) The phase matching condition for the degenerate 4WM process. Phase matching requires that $2k_1 - k_2 - k_3 = 0$. The dashed ring line indicates the endpoints of wave vector k_2 that fulfill phase matching condition. The blue disk of A represents a small phase mismatching regime due to dispersion effect. (b) Spectra of the 4WM wave at different angles. (c, f, i) Input images of the resolution card. (d, g, j, e, h, k) Measured images formed by 4WM wave. The thickness of the glass slide is 1 mm for (d, g, j) and 0.17 mm for (e, h, k). Scale bar, 400 μm .

To experimentally realize such flat lens, we consider the phase matching condition in three-dimensional wave vector space, as shown in Fig. 3(a). The arrow ends of the incident wave vector k_2 that fulfill the phase matching condition in 3D compose a ring in the x-y plane, indicating beams (red beam in Fig. 3a) on the object side with same incident angles respect to pump beams can have their 4WM beams (green beam in Fig. 3a) focused on the image side. Moreover, as mentioned above, for a particular incidence, there exists a small cone of angles nearby (blue disk in the x-y plane in Fig. 3a) that can accept 4WMs due to finite linewidth of ultrafast pulses. By utilizing 4WMs within this region, we achieve a flat lens by probing objects with one color while forming images with others.

First, we experimentally realize optical imaging in a non-collinear configuration as shown in Fig. 1(a),

which explores the small cone spreading caused by pulse wavelength spreading mentioned above (see supplement). With such configuration, the probe beam with wavelength of 1300nm incident on the glass slice at angle $\theta_2 = 7.8^\circ$ in the x-z plane while the pump beam maintains normal incidence. A USAF resolution card is placed in the path of the probe beam, 4.3 cm away from the glass slide. 4WM waves negatively refract and form the image on the other side of the glass slide. After filtering out the probe and pump beams with optical filters, we can obtain the sharpest image out of blurred ones at the distance of around 9.0 cm by moving around the recording CCD camera. Figs. 3(c, f, i) are input images of the resolution card and Figs. 3(d, g, j) are the corresponding images formed by 4WM waves. As comparison, the image of horizontal lines is much clearer than those of vertical ones, because the small angle spreading caused by the object tend to have better phase matching in the y-z plane, closer to the bigger phase matching ring in Fig. 3(a), while in the x-z plane, phase matching by pulse wavelength spreading is less pronounced.

To investigate this dispersion effect further, we replace the glass slide with a thinner one of 0.17 mm thickness. Clearly, color images from Fig. 3 (e, h, k) show dispersive colors ranging from red to green. Also, we perform spectroscopic measurements along the horizontal axis with a thin vertical slit in front of the fiber cable of a spectrometer. The measured spectra in Fig. 3(b) with respective angles of 4WM waves depict sets of spreading spectrum, reaching the peak around $\theta_3 = 3.3^\circ$ under the exact phase matching. Moreover, note that the horizontal field of view is enlarged compared to that out of thick glass slide. Here the thickness of thin glass slide provides an additional phase mismatching factor $k_{\text{glass}} \sim 1/d$ (d is the thickness), that allows $\Delta k = 2k_1 - k_2 - k_3 - k_{\text{glass}}$. Hence thinner lens leads to wider phase matching angle, similar to the process in surface plasmon excitation on metal thin film [17,18]. It is also worth mentioning that (1) the image size is the same as the object (see Fig. 3) as these are one-to-one correspondence with mirror symmetry, no magnification. (2) the image distance Q is related to the object distance P by

$$\frac{Q}{P} = -\frac{\tan\theta_2}{\tan\theta_3} \text{ (the segment in the x-y plane is the same).}$$

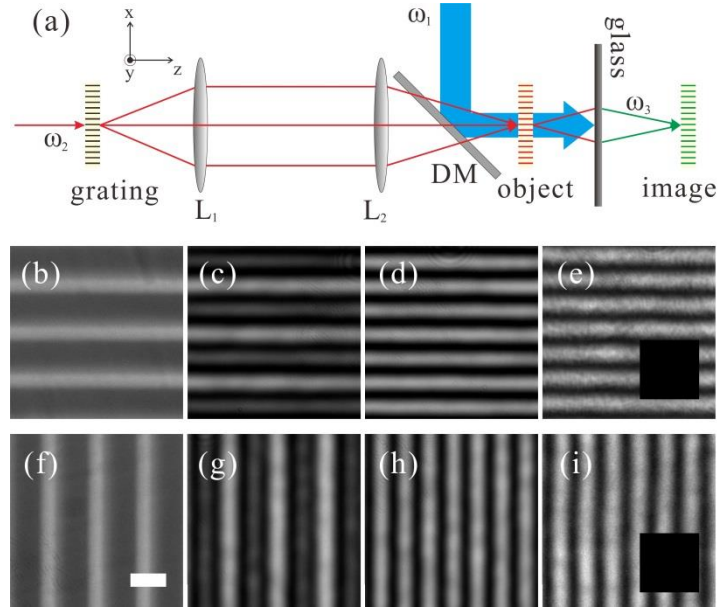


FIG. 4 Imaging a grating (object) by nonlinear negative refraction in collinear configuration. (a) Experimental setup of collinear configuration. L_1, L_2 : lens; DM: dichroic mirror. (b, f) Images of the object. (c, g) Images of the object with grating orders ± 1 and 0. (d, h) Images of the object with grating orders ± 1 . (e, i) Measured images formed by 4WM waves. Insets show images without pump beam. Scale bar, 10 μm .

In order to access the full ring of phase matching on the transverse plane, we construct a collinear configuration where pump and probe beams collinearly propagate, as shown in Fig. 4(a). The pump beam at $\lambda_1 = 800 \text{ nm}$, reflected by a dichroic mirror, incidents on the glass slide normally. The probe beam at $\lambda_2 = 1350 \text{ nm}$ passes through an object (a grating plate) and the image of the object grating is transformed to the front of glass slide by a 4f system using two lenses with focus lengths 4.5cm and 6 cm respectively, in order to avoid the pump beam. The image formed by the 4WM wave at $\lambda_3 = 568 \text{ nm}$ is recorded by a home-build microscope (see supplement). In such way, we can obtain images for both horizontal and vertical direction without the dispersion distortion. Unlike the non-collinear configuration, both vertical and horizontal lines are clear in such collinear configuration by taking advantage of phase matching around the full ring geometry. However these images seems to have finer fringes (Fig. 4 e, i) compared to the original object in Fig. 4 b, f, this is because that 4WM only occurs around the phase matching ring while the probe beam with normal incidence cannot efficiently generate 4WM due to phase mismatch. In Fig. 4, 4WM images are closer to those images of grating without 0 order diffraction (Fig. 4 d, h) as opposed to those with it (Fig. 4 c, g), see supplement. Here resolution of the image is determined by input's numerical aperture (NA), the phase matching cone in our case, which can be estimated as $\frac{0.61\lambda_2}{\sin\theta_2} = 6 \mu\text{m}$ according to Abbe's theory [20]. Since we detect images with a shorter wavelength, ideally we could have a better resolution. Moreover, if combined with nonlinear numerical reconstruction methods in Ref. [21, 22], the resolution can be improved further with enlarged NA.

At last, we would like to comment on the direct implied applications with our flat lens: (1) Infrared (IR)

microscopy, for those fluorescence dyes or biological tissues that emitting IR light, our current configuration can easily convert them into visible light for better detection with more sensitive visible CCD camera, e.g. EMCCD, with a simple glass slide. Compared with flat lens by metal thin film [4] or photonic crystal [5, 23], we can achieve much larger image area up to millimeter scale determined only by pump beams size. (2) Super-resolution imaging is also possible by exploring larger angle cone of phase matching condition and studying the thickness effect of flat lenses. Similar proposals have been posed by using surface plasmon in metallic nanostructures [24, 25], however those may still come along with loss problems, while not ours.

In conclusion, we have experimentally demonstrated a metal-free flat lens using negative refraction by degenerate four-wave mixing with a simple thin glass slide. Our convenient scheme can be served as the fundamental platform for many applications in microscopy and super-resolution imaging in the near future.

Acknowledgements

This work was supported by the National Natural Science Foundation of China (Grant No. 11304201), the National 1000-plan Program (Youth), Shanghai Pujiang Talent Program (Grant No. 12PJ1404700).

Correspondence requests for materials should be addressed to Wenjie Wan (email: wenjie.wan@sjtu.edu.cn)

Reference:

- [1] V.G. Veselago, The electrodynamics of substances with simultaneously negative values of ϵ and μ , *Physics-Usppekhi*, 10 (1968) 509-514.
- [2] J.B. Pendry, Negative refraction makes a perfect lens, *Physical Review Letters*, 85 (2000) 3966-3969.
- [3] J.B. Pendry, Time reversal and negative refraction, *Science*, 322 (2008) 71-73.
- [4] N. Fang, H. Lee, C. Sun, X. Zhang, Sub-diffraction-limited optical imaging with a silver superlens, *Science*, 308 (2005) 534-537.
- [5] P.V. Parimi, W.T.T. Lu, P. Vodo, S. Sridhar, Photonic crystals - Imaging by flat lens using negative refraction, *Nature*, 426 (2003) 404-404.
- [6] J. Valentine, S. Zhang, T. Zentgraf, E. Ulin-Avila, D.A. Genov, G. Bartal, X. Zhang, Three-dimensional optical metamaterial with a negative refractive index, *Nature*, 455 (2008) 376-U332.
- [7] Z. Liu, H. Lee, Y. Xiong, C. Sun, X. Zhang, Far-field optical hyperlens magnifying sub-diffraction-limited objects. *Science* 315, 1686
- [8] S. Zhang, W.J. Fan, N.C. Panoiu, K.J. Malloy, R.M. Osgood, S.R.J. Brueck, Experimental demonstration of near-infrared negative-index metamaterials, *Physical Review Letters*, 95 (2005).
- [9] H.J. Lezec, J.A. Dionne, H.A. Atwater, Negative refraction at visible frequencies, *Science*, 316 (2007) 430-432.
- [10] C.M. Soukoulis, S. Linden, M. Wegener, Negative refractive index at optical wavelengths, *Science*, 315 (2007) 47-49.
- [11] S. Maslovski, S. Tretyakov, Phase conjugation and perfect lensing, *Journal of Applied Physics*, 94 (2003) 4241-4243.
- [12] A. Aubry, J.B. Pendry, Mimicking a negative refractive slab by combining two phase conjugators, *J Opt Soc Am B*, 27 (2010) 72-84.
- [13] S. Palomba, S. Zhang, Y. Park, G. Bartal, X. Yin, X. Zhang, Optical negative refraction by four-wave mixing in thin metallic

nanostructures, *Nature Materials*, 11 (2011) 34-38.

[14] H. Harutyunyan, R. Beams, L. Novotny, Controllable optical negative refraction and phase conjugation in graphite thin films, *Nature Physics*, 9 (2013) 423-425.

[15] A.R. Katko, S. Gu, J.P. Barrett, B.I. Popa, G. Shvets, S.A. Cummer, Phase Conjugation and Negative Refraction using Nonlinear Active Metamaterials, *Physical Review Letters*, 105 (2010).

[16] R. W. Boyd, *Nonlinear optics*, Third Edition (Academic Press, 2008).

[17] J. Renger, R. Quidant, N. van Hulst, S. Palomba, L. Novotny, Free-Space Excitation of Propagating Surface Plasmon Polaritons by Nonlinear Four-Wave Mixing, *Physical Review Letters*, 103 (2009).

[18] J. Renger, R. Quidant, N. Van Hulst, L. Novotny, Surface-enhanced nonlinear four-wave mixing, *Physical Review Letters*, 104 (2010) 46803.

[19] H. Harutyunyan, S. Palomba, J. Renger, R. Quidant, L. Novotny, Nonlinear Dark-Field Microscopy, *Nano letters*, 10 (2010) 5076-5079.

[20] E. Abbe, *Arch. Mikrosk. Anat.* 9, 413 (1873).

[21] C. Barsi, W.J. Wan, J.W. Fleischer, Imaging through nonlinear media using digital holography, *Nature Photonics*, 3 (2009) 211-215.

[22] C. Barsi, J.W. Fleischer, Nonlinear Abbe theory, *Nature Photonics*, (2013).

[23] N. Fabre, L. Lalouat, B. Cluzel, X. Melique, D. Lippens, F. de Fornel, O. Vanbesien, Optical near-field microscopy of light focusing through a photonic crystal flat lens, *Physical Review Letters*, 101 (2008).

[24] P.Y. Chen, A. Alu, Subwavelength Imaging Using Phase-Conjugating Nonlinear Nanoantenna Arrays, *Nano letters*, 11 (2011) 5514-5518.

[25] B. Simkhovich, G. Bartal, Plasmon-Enhanced Four-Wave Mixing for Superresolution Applications, *Physical Review Letters*, 112 (2014).